Parametric X-Rays at FAST

Tanaji Sen
Fermi National Laboratory, Batavia, IL 60510, USA

ABSTRACT

We discuss the generation of parametric X-rays (PXR) in the photoinjector at the new FAST facility at Fermilab. Detailed calculations of the intensity spectrum, energy and angular widths and spectral brilliance with a diamond crystal are presented. We also report on expected results with PXR generated while the beam is channeling. A new goniometer with several ports could allow the simultaneous detection of PXR at multiple energies.

MOTIVATION

10 keV X-rays	Beam Energy
Synchrotron Radiation	3 GeV
Transition Radiation	300 MeV
Compton Scattering	22 MeV
Channeling Radiation	10 MeV
Parametric Radiation	5.7 MeV

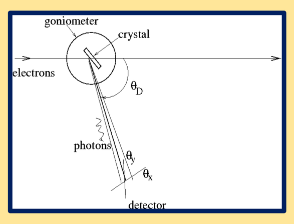

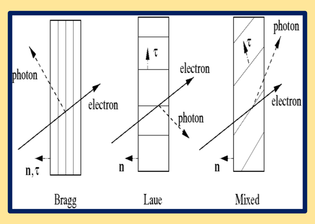

Parameter	Value
Beam energy	50 [MeV]
Bunch charge	20 [pC]
Length of a macropulse	1 [ms]
Number of bunches/macropulse	2000
Macropulse repetition rate	5 [Hz]
Crystal, thickness	Diamond, 168 [μm]

- Emitted at large angles from the beam direction. Differentiates it from channeling, bremsstrahlung
- X-ray energy is independent of beam energy
- Tunable by changing crystal orientation
- Narrow line width. Typically ~ 1%
- Lower background from other sources, especially at large angles.
- Can be produced while channeling
- Multiple X-ray energies at once.

PXR SPECTRUM

$$E = \hbar c \frac{g\sin(\theta_B+\alpha)}{2\sin^2((\theta_D+\alpha)/2)} \overset{\theta_D=2\theta_B,\alpha=0}{\longrightarrow} \hbar c \frac{g}{2\sin\theta_B}$$

- PXR energy depends on the lattice spacing, Bragg angle and angle of detection.

$$\frac{d^3N}{d\omega d\theta_x d\theta_y} = \frac{\alpha_f}{4\pi}\frac{\omega}{c} f_{geo}(\hat{n},\hat{v},\hat{\Omega}) e^{-M(g)} \frac{|\chi_g(\omega)|^2}{\sin^2\theta_B}\left[\frac{\theta_x^2\cos^2 2\theta_B+\theta_y^2}{[\theta_x^2+\theta_y^2+\theta_{ph}^2]^2}\right]\delta(\omega - m\omega_B)$$

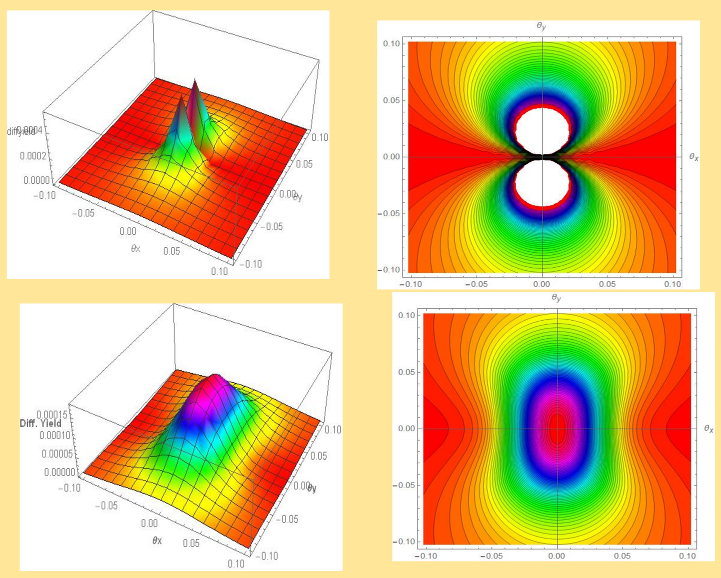

- Photon intensity depends on path length in crystal, angle between lattice plane and normal to surface
- Also on the susceptibility, crystal structure factor. Only some planes allowed
- Angular spectrum is broadened by multiple scattering, angular resolution

LINEWIDTH

$$\left(\frac{\Delta E}{E}\right)_{geom} = \frac{1}{R}\left[\left(\frac{\Delta x_{det}\sigma_x'}{2\sin^2\theta_B}\right)^2 + \cot^2\theta_B\left\{(\sigma_x\sin(\theta_B+\zeta))^2 + \left(t\frac{\sin 2\theta_B}{\sin(\theta_B+\zeta)}\right)^2 + (\Delta x_{det})^2\right.\right.$$

$$\left(\frac{dN}{d\theta_x}\right)_{MS} = \mathcal{A}\int\int\int \frac{dz\,d\phi_x\,d\theta_y}{E(\theta_x+\phi_x)[\hat{n}\cdot\hat{v}]\sigma_x'(z)} \exp\left[-\frac{z}{L_a|\hat{n}\cdot\hat{\Omega}|} - \frac{\phi_x^2}{2\sigma_x'^2}\right]\frac{\theta_x^2\cos^2 2\theta_B+\theta_y^2}{[\theta_x^2+\theta_y^2+\theta_{ph}^2]^2}$$

$$\langle E\rangle = \frac{\int E(dN/d\theta_x)_{MS}d\theta_x}{\int(dN/d\theta_x)_{MS}d\theta_x}, \quad \sigma_{E,MS}^2 = \langle E^2\rangle - \langle E\rangle^2$$

- Smaller linewidth increases brilliance, important for applications
- Geometric effects and multiple scattering are largest effects
- Main geometric effects from beam size and the detector width.
- Multiple scattering effects are found analytically.
- Theory agrees well with previous experimental results

YIELD, SPECTRAL BRILLIANCE

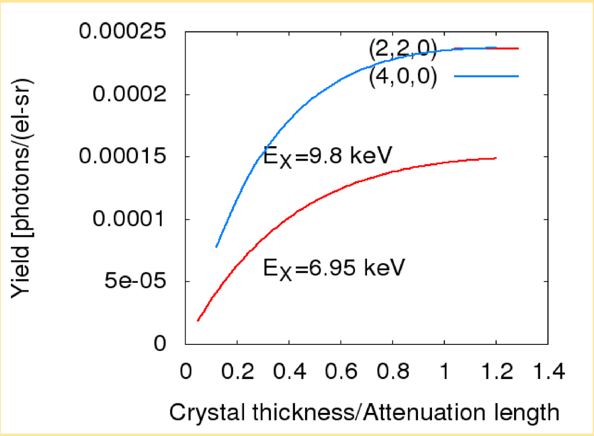

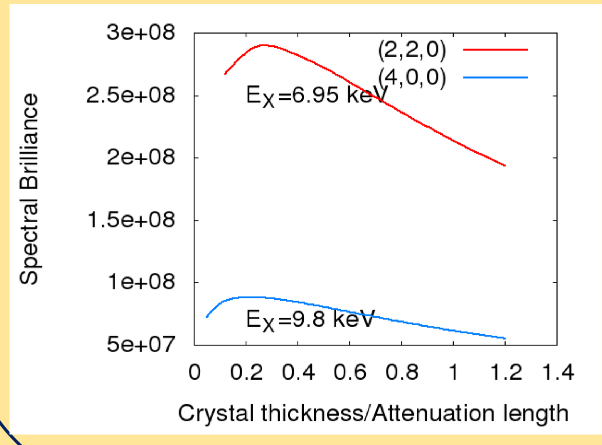

Plane	X-ray energy [keV]	$L_{a,C}$ [cm]	$L_{a,air}$ [cm]	Attenuation in air	Yield [photons/el-sr]	ΔE [eV]
(1,1,1)	4.26	0.0097	12.72	3.8×10^{-4}	3.7×10^{-7}	59
(2,2,0)	6.95	0.043	57.2	0.17	9.9×10^{-5}	93
(4,0,0)	9.83	0.120	144.9	0.50	8.8×10^{-5}	131

- Same goniometer as used for channeling. 90° port determines Bragg angle= 45°
- Photon absorption in 1m of air included.
- Brilliance averaged over emittance growth.
- Yield saturates at crystal thickness L_C=1.2 L_a; brilliance at L_C = 0.25 L_a

PXR WHILE CHANNELING

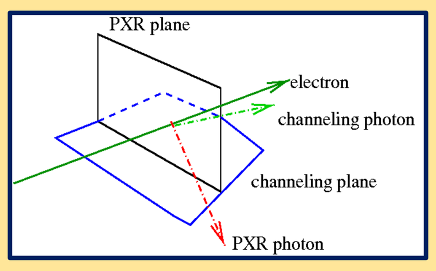

$$\begin{aligned}
\frac{d^2N}{d\theta_x\theta_y}|_{PXRC} &= \frac{d^2N}{d\theta_x\theta_y}|_{PXR}\sum_n^{N_B} P_n|F_{nn}|^2 \\
\langle P_n\rangle &= \frac{1}{\sqrt{2\pi}\sigma_x'}\frac{1}{d_p}\langle\int d\phi_{x,0}e^{-\frac{\phi_{x,0}^2}{2(\sigma_x')^2}}|\int_{-d_p/2}^{d_p/2}e^{-ik\phi_{x,0}x}\psi_{n,K_C}(x)dx|^2\rangle_{K_C} \\
\langle|F_{nn}(\theta_x)|^2\rangle &= \frac{1}{d_p^2}\langle|\int_{-d_p/2}^{d_p/2}\psi_{n,K_C}^*(x)e^{-i\frac{\omega_B\theta_x x}{c}}\psi_{n,K_C}(x)dx|^2\rangle_{K_C} \\
\delta &= 1-\sum^{N_B}\langle P_n\rangle\langle|F_{nn}|^2\rangle
\end{aligned}$$

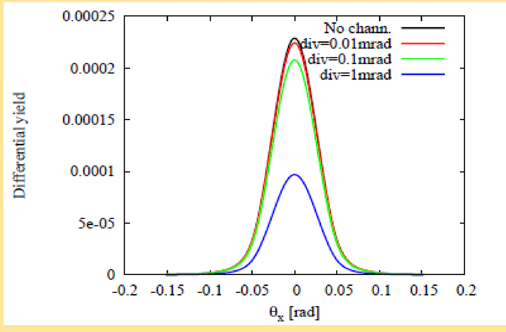

Plane	σ'[mrad]	Yield	Spect. Brill.
(2,0,$\bar{2}$)	0.01	0.38	35.1
	0.1	0.35	1.9×10^5
	1.0	0.16	1.8×10^8

Y: 10^{-4} phot/(e^- - sr)
S.B: phot/(mm-mrad)^{2}0.1%BW

- PXRC is PXR emitted by channeled electrons and making intra-band transitions
- PXRC along (2,0,-2) plane, channeling along (1,1,0) plane without crystal rotations
- Yield decreases with beam divergence, but spectral brilliance increases

NEW GONIOMETER

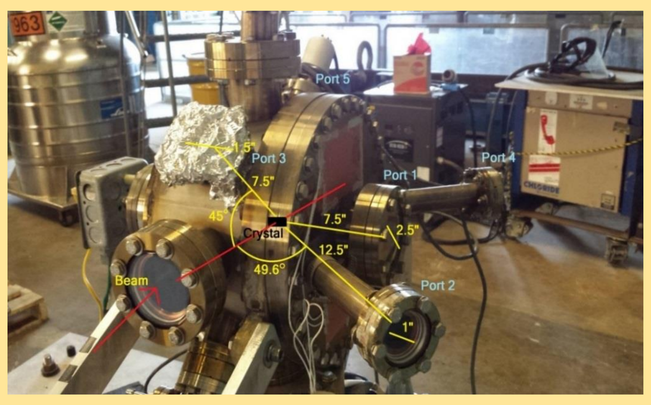

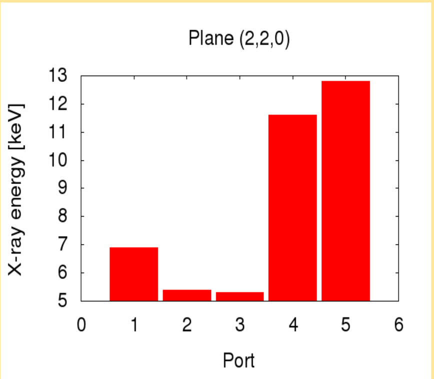

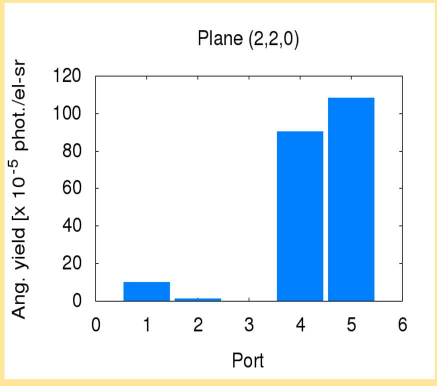

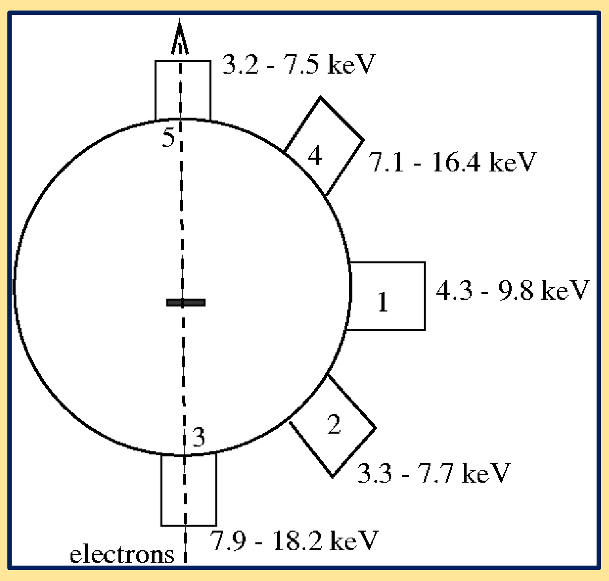

Port	Plane 111			Plane 220		
	Energy	t/L_a	Sp. Br. [$\times10^8$]	Energy	t/L_a	Sp. Br. [$\times10^8$]
4	7.1	0.36	5.5	11.6	0.09	2.2
5	7.9	0.26	5.7	12.8	0.07	2.1
Port	**Plane 311**			**Plane 400**		
	Energy	t/L_a	Sp. Br. [$\times10^8$]	Energy	t/L_a	Sp. Br. [$\times10^8$]
4	13.6	0.06	0.59	16.4	0.04	0.59
5	15.1	0.05	0.57	18.2	0.03	0.56

- X-ray energies from 3 – 18 keV
- Yield, brilliance highest at ports 4, 5
- Plane (1,1,1) has highest brilliance
- Larger thickness increases brilliance for higher energy X-rays

APPLICATIONS

- Low emittance beam would give higher brilliance PXR
- Phase contrast imaging with better resolution
- Sub-ps X-ray pulses with a slit mask in chicane